Journal of Molecular Catalysis A: Chemical 418 (2016) 86–94

Contents lists available at ScienceDirect

Journal of Molecular Catalysis A: Chemical

journal homepage: www.elsevier.com/locate/molcata

Shape selectivity of beta and MCM-49 zeolites in liquid-phase alkylation of benzene with ethylene

Yanchun Shi, Enhui Xing, Wenhua Xie, Fengmei Zhang*, Xuhong Mu, Xingtian Shu

State Key Laboratory of Catalytic Materials and Reaction Engineering, Research Institute of Petroleum Processing, Sinopec, Beijing 100083, China

ARTICLE INFO

Article history:
Received 3 December 2015
Received in revised form 24 March 2016
Accepted 25 March 2016
Available online 26 March 2016

Keywords:
Shape selectivity
Beta
MCM-49
Liquid-phase alkylation
Ethylbenzene

ABSTRACT

NH_3, pyridine and 2,4,6-trimethyl-pyridine were selected as the base probes to characterize the different pore acidity of H-beta and H-MCM-49 zeolites, revealing the essence in their catalytic performance from the view of shape selectivity in different pore systems. Based on the size of base probes, reactants, product, transition states and pore channels, the difference in catalytic performance over H-beta and H-MCM-49 was investigated. Easy diffusion of reactants into and long diffusion distance for ethylbenzene escaping out of confined space within beta are the main reason for superior activity and poorer ethylbenzene (EB) selectivity. As for H-MCM-49, acid sites located in 10 MR channels contributed little to the formation of EB due to transition state selectivity; Acid sites located in 12 MR cups on the outer surface with little restriction on the diffusion of reactant/product toward/from the active centers were the major active centers for EB formation, which could be detected by 2,4,6-trimethyl-pyridine; There was diffusion limitation on reactant/product in 12 MR supercages through 10 MR windows to influence activity/selectivity. The enhancement in activity and selectivity in liquid-phase alkylation of benzene with ethylene over MWW zeolites should be mainly focused on transforming confined 12 MR supercages into 12 MR cups with improved openness.

1. Introduction

Zeolites have been widely utilized in the refining and petrochemical processes with superior selectivity, environmental benign and easy reproducibility in catalytic reactions, based upon their framework structure with ordered micropores and adjustable acidic property dispersed within regular pores [1,2]. Because of their confined space around active centers and restricted access to and escape from the internal surface, zeolites facilitate only certain reactions between molecules having specific dimensions, so-called the concept of "shape-selective catalysis" by Weisz, and there are well known as reactant selectivity, transition state selectivity and product selectivity according to sizes of reactant/transition state/product, respectively [3–5]. Based upon mass transport limitation (reactant/product), molecules that are suitable to zeolitic pores could diffuse freely within the inner pores and access/escape to/from the active centers, which contributes to improve activity and selectivity over zeolite catalysts. Additionally transition state control of reactions could be significantly enhanced due to smart fitting between dimensions of transition states and confined spaces within zeolites. Shape-selective catalysis of zeolite has been extensively proven and industrialized in petro-refining and petrochemical processes [1–8].

Catalytic performances of zeolite-based catalysts are influenced but not limited by their morphology, textual properties and chemical compositions, especially determined by the match between zeolite pores/spaces and the sizes of reactant/transition-state/product [9–12]. As well known, the liquid-phase alkylation of benzene with ethylene is a well-established process in both academic research and the petrochemical industry, in which *BEA and MWW zeolites have been proven to be superior catalysts because of easy separation, low corrosion, valuable activity, high selectivity and long catalytic life [13–21]. Generally speaking, *BEA zeolites show better activity of ethylene conversion; on the contrary, MWW zeolites exhibit higher selectivity of ethylbenzene (EB) especially at lower molar ratio of benzene/ethylene. *BEA zeolite has a three-dimensional pore system consisting of 12-membered ring (MR) channels (0.66 nm × 0.67 nm & 0.56 nm × 0.56 nm), while MWW zeolites have three complex pore systems: 12 MR cups (half supercages 0.71 nm × 0.71 nm × 0.91 nm) on the external surface, the interlayer12 MR supercages (0.71 nm outside diameter × 1.82 nm height) through10 MR opening windows (0.41 nm × 0.54 nm & 0.41 nm × 0.59 nm), and the intralayer two-

* Corresponding author at: Research Institute of Petroleum Processing Sinopec, Xueyuan Road 18, Beijing, China.
E-mail address: zhangfm.ripp@sinopec.com (F. Zhang).

http://dx.doi.org/10.1016/j.molcata.2016.03.039
1381-1169/

dimensional sinusoidal 10 MR pores (0.41 nm × 0.54 nm) [22–25]. As solid acidic catalysts, acid sites dispersed in different pore system of *BEA and MWW zeolites would derive the issue on accessibility of active centers, diffusion lengths for reactant/product and reaction spaces for transition state, determining the apparent catalytic performances in liquid-phase alkylation of benzene with ethylene.

Based upon reactant selectivity, the acidity of H-type zeolites are usually determined by base probes with different molecule sizes, such as NH_3 (kinetic diameter 0.26 nm) in TPD characterization and pyridine (kinetic diameter 0.58 nm) in FTIR experiments. Both NH_3 and pyridine are effective to access acid sites located in micro pores, however they can offer little information about acid sites in different pore systems and on the internal/external surface, especially for MWW zeolites with three different pore systems. It has been well reported that 2,4,6-trimethyl-pyridine (kinetic diameter 0.74 nm) was used to detect the acid sites in 12 MR cups on the outer surface of MWW zeolites, because 2,4,6-trimethyl-pyridine fit snugly into the 12 MR cups but not penetrate 10 MR pores and windows [20,26–28]. Furthermore, there is little reaction in the 2,4,6-trimethyl-pyridine-doped runs confirming that the ethylation occurred almost exclusively in the 12 MR cups on the outer surface of MWW zeolites.

As common recognized, H-type zeolites show different acidity with different base probes due to reactant selectivity via gas-solid heterogonous reaction, which may have a similar tendency in liquid-solid heterogonous reaction. The relationship between guest molecules (base probes, reactants, transitional states and products) and the sizes of zeolite pore systems has always been interesting and challenging topic for zeolite-catalyzed reaction, which needs comprehensive consideration on distribution and accessibility of acid sites in different pore systems to tailor their catalytic performances. Therefore NH_3, pyridine and 2,4,6-trimethyl-pyridine were selected as the base probes to characterize accessibility of the different pore acid sites over H-beta and H-MCM-49 zeolites in this paper. Focusing on the perspective of shape-selective catalysis, we anticipate to reveal potential essence of different liquid-phase alkylation performances over *BEA and MWW zeolites, and propose corresponding strategies to enhance ethylene conversion without loss of EB selectivity over *BEA and MWW zeolites respectively.

2. Experimental

2.1. Preparation of beta, MCM-49 zeolites and H-type catalysts

2.1.1. Synthesis of MCM-49 zeolites

Beta zeolite was provided by Research Institute of Petroleum Processing, Sinopec. All materials such as solid silica gel, $NaAlO_2$, NaOH, hexamethyleneimine (HMI), aniline (AN) and deionized water were used as purchased. Detailed conditions of synthesis are provided in Table 1. The hydrothermal synthesis of MCM-49 was carried out for 72 h at 145 °C in a stirred vessel (15 Hz) [29,30]. The products were filtrated, washed with deionized water until pH = 7, and dried at 100 °C overnight. Samples were calcined at 550 °C in ambient air for 6 h in a muffle furnace to remove organics.

2.1.2. H-type zeolites

Usually Na_2O content of H-type catalysts for liquid-phase alkylation of benzene with ethylene are required below 0.05 wt.%. H-beta (Na_2O <0.01 wt.%) was obtained via direct calcination of as-synthesized beta without further ion-exchange. NH_4-MCM-49 was first prepared by twice liquid-phase ion-exchange of Na-MCM-49 with NH_4NO_3 solution at 90 °C for 2 h to reduce Na_2O content below 0.05 wt.%. The mass ratio composition of MWW zeolites, NH_4NO_3, and deionized water was: 1:1:20. The products were filtrated, washed with deionized water until pH = 7, and dried at 100 °C overnight. Samples were calcined at 550 °C in ambient air for 6 h in a muffle furnace to remove organics and decompose NH_4^+ to form H-type zeolites.

2.1.3. H-type catalysts

The as-synthesized beta and NH_4-MCM-49 zeolites were mixed with Al_2O_3 (30 wt.%) and extruded. Al_2O_3 showed almost no activity for the liquid-phase alkylation of benzene with ethylene and was used as binder to increase the mechanical strength of catalysts. The extruded catalysts were then crushed, and the −16/+20 mesh fraction was collected and subjected to calcination at 550 °C for 6 h to obtain corresponding H-type catalysts.

2.2. Characterization of beta and MCM-49 zeolites

X-ray diffraction (XRD) patterns of samples were collected on a D/MAX-III X-ray diffractometer (Rigaku Corporation, Japan) with filtered Cu K α radiation at a tube current of 35 mA and a voltage of 35 kV. The scanning range of 2θ was 5–35°. The crystal morphology was measured on a FEI Quanta scanning electron microscope (SEM). The elemental analyses of the solids were performed on an X-ray fluorescence (XRF) spectrometer MagiX (Philips). Nitrogen adsorption-desorption isotherms were recorded on a Micromeritics ASAP 2010 instrument. The samples were first out-gassed under vacuum at 363 K for 1 h and at 623 K for 15 h. The total surface area was obtained by application of the BET equation using the relative pressure range of 0.05–0.16 in the nitrogen adsorption isotherm as range of linearity (using a molecular cross-sectional area for N_2 of 0.162 nm^2). The micropore volume was calculated by the t-plot method.

The acidity of H-type zeolites was measured by temperature programmed desorption (TPD) and Fourier transform infrared spectrometer (FTIR),using ammonia(NH_3) and pyridine/2,4,6-trimethyl-pyridine as probe molecules, respectively. NH_3-TPDwas carried out on an Autochem II 2920 unit equipped with a thermal conductivity detector. For FTIR spectroscopy of adsorbed probe molecules (pyridine and 2,4,6-trimethyl-pyridine), all samples were pressed into self-supporting wafers and measured in transmission mode in an FTS3O00 FTIR spectrometer by 64 scans with a resolution of 4 cm^{-1}. Prior to the measurements, each sample was dehydrated under vacuum 10^{-3} Pa at 350 °C for1 h, and then cooled to 50 °C for pyridine adsorption. The IR spectra of the samples before pyridine adsorption were recorded at different temperatures (200 and 350 °C), and after adsorbing pyridine for 10 s, the samples were purged under vacuum 10^{-3} Pa to higher temperature at a heating rate of 10 °C min^{-1}. Then the IR spectra of pyridine on samples were recorded at different temperatures (200 and 350 °C), while IR spectra of pyridine was collected at 200 °C. All the spectra given in this work were differential spectra. The number of Brønsted and Lewis acid sites was calculated according to adsorbed pyridine IR peak area, and the number of acid sites by 2,4,6-trimethyl-pyridine was calculated based upon adsorbed 2,4,6-trimethyl-pyridine IR peak height.

$^{29}Si/^{27}Al$ MAS NMR experiments were performed on a Bruker AVANCE III 500WB/600WB spectrometer at a resonance frequency of 99.3/156.4 MHz using a 7/4 mm double-resonance MAS probe with a recycle delay of 4/1 s respectively. The magic-angle spinning rate was 5/13 kHz in all experiments, and a typical length of 1.8/0.4 μs was adopted for $^{29}Si/^{27}Al$ resonance respectively. The chemical shift of $^{29}Si/^{27}Al$ was referenced to tetramethylsilane (TMS)/1 M aqueous Al $(NO_3)_3$ respectively.

Table 1
Synthetic condition of beta and MCM-49.

Samples	Si source	Feeding composition (mol/mol)						Temperature (°C)	Time (h)
		SiO_2/Al_2O_3	$NaOH/SiO_2$	H_2O/SiO_2	$TEAOH/SiO_2$	HMI/SiO_2	AN/SiO_2		
Beta	Si-Al gel	25	–	7	0.1	–	–	120/145	12/36
MCM-49	Solid silica gel	25	0.18	15	–	0.1	0.2	145	72

2.3. Liquid-phase alkylation of benzene with ethylene

The liquid-phase alkylation of benzene with ethylene was carried out in a stainless-steel fixed bed reactor. The catalyst (8 mL) was placed in the center of the reactor and purged with nitrogen. Benzene was pumped into the reactor to fill the bed fully under reaction pressure, and then the temperature was raised to 200 °C before ethylene was introduced. The alkylation conditions were as follows: pressure of 3.5 MPa, weight hourly space velocity (WHSV) of benzene of 3 h^{-1}, the molar ratio of benzene/ethylene 12/1, and 200–260 °C of temperature. At each temperature the reaction was given at least 15 h to reach a steady state condition before samples were collected for analysis. The reaction products were analyzed by an Agilent 6890 gas chromatograph (GC) equipped with a flame ionization detector and a capillary column. It is well known that the alkylation of benzene with ethylene is a consecutive reaction, and the reaction products were made up of EB, *para*-diethylbenzene (*p*-DEB), *ortho*-diethylbenzene (*o*-DEB), *meta*-diethylbenzene (*m*-DEB), triethylbenzenes (TEB), and other by-products (diphenylethane) in our work. The ethylene conversion, EB selectivity, DEB selectivity, DEB selectivity distribution and ethylation selectivity were calculated based upon formulas as follows:

$$H = x_{EB}/M_{EB} + 2x_{DEB}/M_{DEB} + 3x_{TEB}/M_{TEB} + x_{diphenylethane}/M_{diphenylethane};$$

$$x_{DEB} = x_{p\text{-}DEB} + x_{o\text{-}DEB} + x_{m\text{-}DEB};$$

M: molar mass (g/mol);
x: mass percentage concentration (wt.%) from GC analysis;
H: molar number percentage concentration (mol%) of ethyl;

$$\text{Ethylene conversion}(\%): C_{ethylene} = H/(H + x_{ethylene}/M_{ethylene}) \times 100\% \quad (1)$$

$$\text{EB selectivity}(\%): S_{EB} = x_{EB}/(x_{EB} + x_{DEB} + x_{TEB} + x_{diphenylethane}) \times 100\% \quad (2)$$

$$\text{DEB selectivity}(\%): S_{DEB} = x_{DEB}/(x_{EB} + x_{DEB} + x_{TEB} + x_{diphenylethane}) \times 100\% \quad (3)$$

$$\text{TEB selectivity}(\%): S_{TEB} = x_{TEB}/(x_{EB} + x_{DEB} + x_{TEB} + x_{diphenylethane}) \times 100\% \quad (4)$$

$$\text{Ethylation selectivity}(\%): S_{ethyl} = (x_{EB}/M_{EB} + 2x_{DEB}/M_{DEB} + 3x_{TEB}/M_{TEB})/H \times 100\% \quad (5)$$

3. Results and discussion

3.1. Characterization of beta and MCM-49 zeolites

Both beta and MCM-49 zeolites were intentionally synthesized with the feeding SiO_2/Al_2O_3 molar ratio at 25 to diminish the effects of framework compositions. Tetraethylammonium hydroxide (TEAOH) was used as the structure-directing agent (SDA) to synthesize beta zeolite. Temperature-controlled phase transfer hydrothermal synthesis of MCM-49 was achieved with HMI as a SDA coupled with aniline as structure-promoting agent [29,30]. XRD patterns of as-synthesized/calcined beta and MCM-49 zeolites are shown in Fig. 1, which agreed well with the published data without any diffraction peaks of other competing phases [23,36]. As can be seen from the SEM images shown in Fig. 2, beta showed much smaller particles with diameters at about 50 nm, while MCM-49 was of rose-like shape at about 2–5 μm and 20–40 nm in thickness.

Fig. 3 presents the $^{29}Si/^{27}Al$ MAS NMR spectra of as-synthesized/calcined beta and MCM-49 zeolites. The resonances

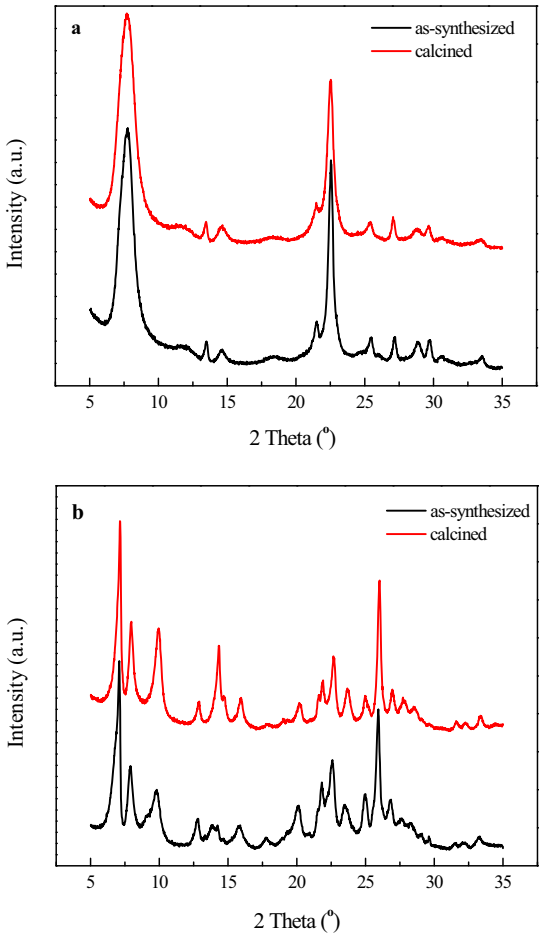

Fig. 1. XRD patterns of as-synthesized/calcined beta (a) and MCM-49 (b).

Table 2
Textural properties of H-type zeolites.

Samples	Na_2O wt%	SiO_2/Al_2O_3	S_{BET} (m^2/g)	S_{micro} (m^2/g)	S_{ext} (m^2/g)	V_{micro} (cm^3/g)	V_{total} (cm^3/g)
H-beta	<0.01	25	571	471	100	0.22	0.62
H-MCM-49	0.02	23	485	410	75	0.19	0.56

S_{BET} were calculated by BET method. Micropore volume and surface area were calculated by *t*-plot method. $S_{external} = S_{BET} - S_{micro.}$

of MCM-49 were similar to those presented in previous publications with six resonances at about −100, −105, −110, −110, −115 and −119 ppm, which were mainly associated with Si sites of MWW zeolites as follows: −100 ppm ~ Si (1Al) and −105 ppm to −119 ppm ~ Si (0Al) [31–35]. Usually the resonances at about −110, −110 and −115 overlapped. While for beta, the resonance at about −103 ppm was ascribed to Si (1Al), and −105 to −119 ppm to Si (0Al) [36]. As for ^{27}Al MAS NMR spectra of MCM-49 were both comprised of at least two tetrahedral Al resonances centered at ~50 and ~56 ppm. Upon calcination, the shoulder at ~49 ppm was further reduced while the resonance at ~60 ppm also appeared as a shoulder and was more visible. A sharp peak at ~0 ppm due to octahedral aluminum can be clearly observed, indicating that calcination caused dealumination to some extent [23]. The framework Al resonance at ~55 ppm of as-synthesized beta was divided into two peaks located at ~56 and ~54 ppm after calcination, causing the formation of extra-framework Al with a sharp resonance at ~0 ppm and a broad resonance at ~5 ppm.

The compositions, BET surface areas and pore volumes of H-type zeolites are shown in Table 2. The SiO_2/Al_2O_3 ratio of H-beta was identical to that of feeding composition at 25, however the H-MCM-49 showed a slightly lower SiO_2/Al_2O_3 ratio at 23 than the feeding composition at 25. H-beta with 12 MR channels showed larger surface areas (both micro and external) and pore volumes than H-MCM-49 with 12 MR and 10 MR pore systems. It is reasonable to conclude that larger pore systems surely lead to the increase in adsorption capability of N_2 (kinetic diameter 0.36 nm), which may be less restriction and larger space for reactant/transition state/product than H-MCM-49.

3.2. Acidity of H-beta and H-MCM-49 zeolites

H-MCM-49 had lower SiO_2/Al_2O_3 ratio at 23 than H-beta (SiO_2/Al_2O_3 = 25), indicating that H-MCM-49 may exhibit a higher Al content and acidic density. However, not all of these acid sites (or active centers) could be accessed by base probes and more importantly cannot be accessed by reactants during catalytic reactions. In this section, base probes with different molecule sizes were selected to detect the accessibility of acid sites in different pore system of these two zeolites. NH_3 was selected based upon little diffusion restriction into *BEA and MWW pore systems. Pyridine with identical kinetic diameter as benzene (0.58 nm) was selected to reveal reactant selectivity. 2,4,6-Trimethyl-pyridine with size larger than benzene and smaller than the sum of benzene and ethylene (0.39 nm), has similar size to the transition state of benzene ethylation to indicate the transition state selectivity.

Fig. 4 shows NH_3-TPD curves of H-beta and H-MCM-49 zeolites. Obviously, H-MCM-49 had more weak and strong acid sites due to its slightly lower SiO_2/Al_2O_3 ratio. While Py-FTIR analysis (Table 3) shows reverse results of total acid sites: H-beta (423 μmol g^{-1} of Brønsted acid sites and 271 μmol g^{-1} of Lewis acid sites at 200 °C; 396 μmol g^{-1} of Brønsted acid sites and 227 μmol g^{-1} of Lewis acid sites at 350 °C) showed a little higher acidic concentration than H-MCM-49 (402 μmol g^{-1} of Brønsted acid sites and 189 μmol g^{-1} of Lewis acid sites at 200 °C; 375 μmol g^{-1} of Brønsted acid sites and 168 μmol g^{-1} of Lewis acid sites at 350 °C). NH_3 molecule has smaller kinetic diameter to present little diffusion restriction into inner channels of H-beta and H-MCM-49 zeolites. The restriction of MCM-49 windows on its assessment of some acid sites may show less acid sites detected by pyridine with larger molecule size. Because of 12 MR pore system, H-beta has larger space for pyridine to access acid sites than H-MCM-49 with 12 MR and 10 MR pore systems. An excellent summary of Brønsted and Lewis acid sites concentration of MWW zeolites was reported by Gil et al. [37]. There are some differences in the concentration of acid sites. Main reason lied in the absorption coefficients in different group.

According to published results, 2,4,6-trimethyl-pyridineis a bulky base to distinguish acid sites on the inner pores and outer surface areas, however it failed in characterizing internal/external acidity of H-beta with 12 MR pore system [20,26–28]. Fig. 5 shows spectra of H-beta and H-MCM-49 before/after 2,4,6-trimethyl-pyridine adsorption. 2,4,6-Trimethyl-pyridine adsorbed on Brønsted and Lewis acid sites gave the band at about ~1650 and ~1633 cm^{-1} [38]. What's more, there were obvious physi-

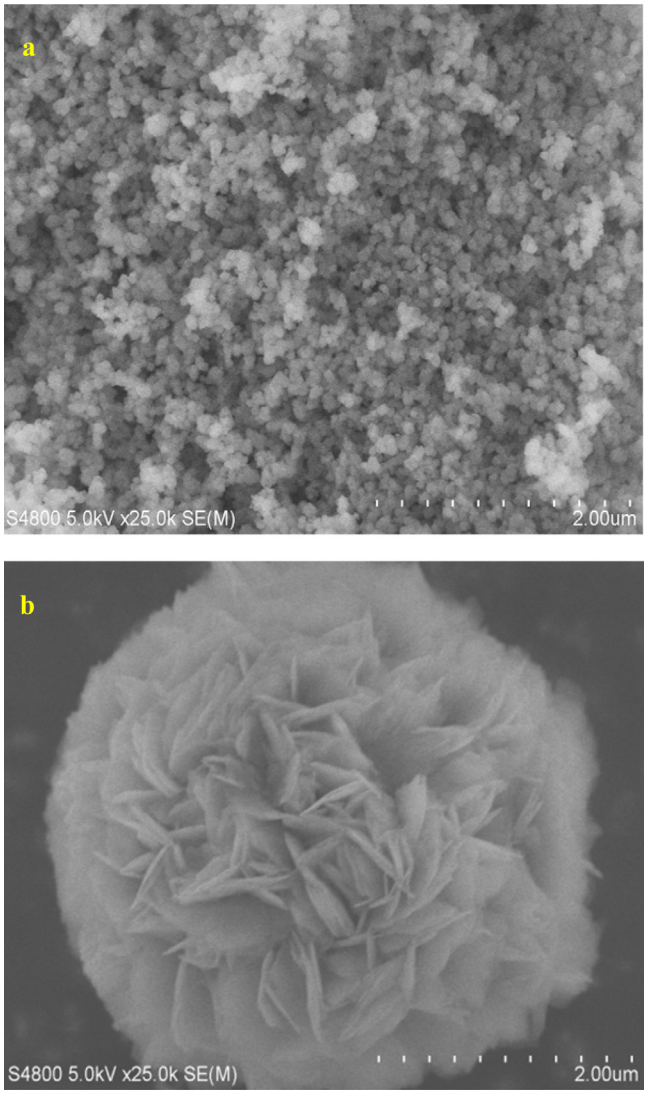

Fig. 2. SEM images H-beta (a) and H-MCM-49 (b).

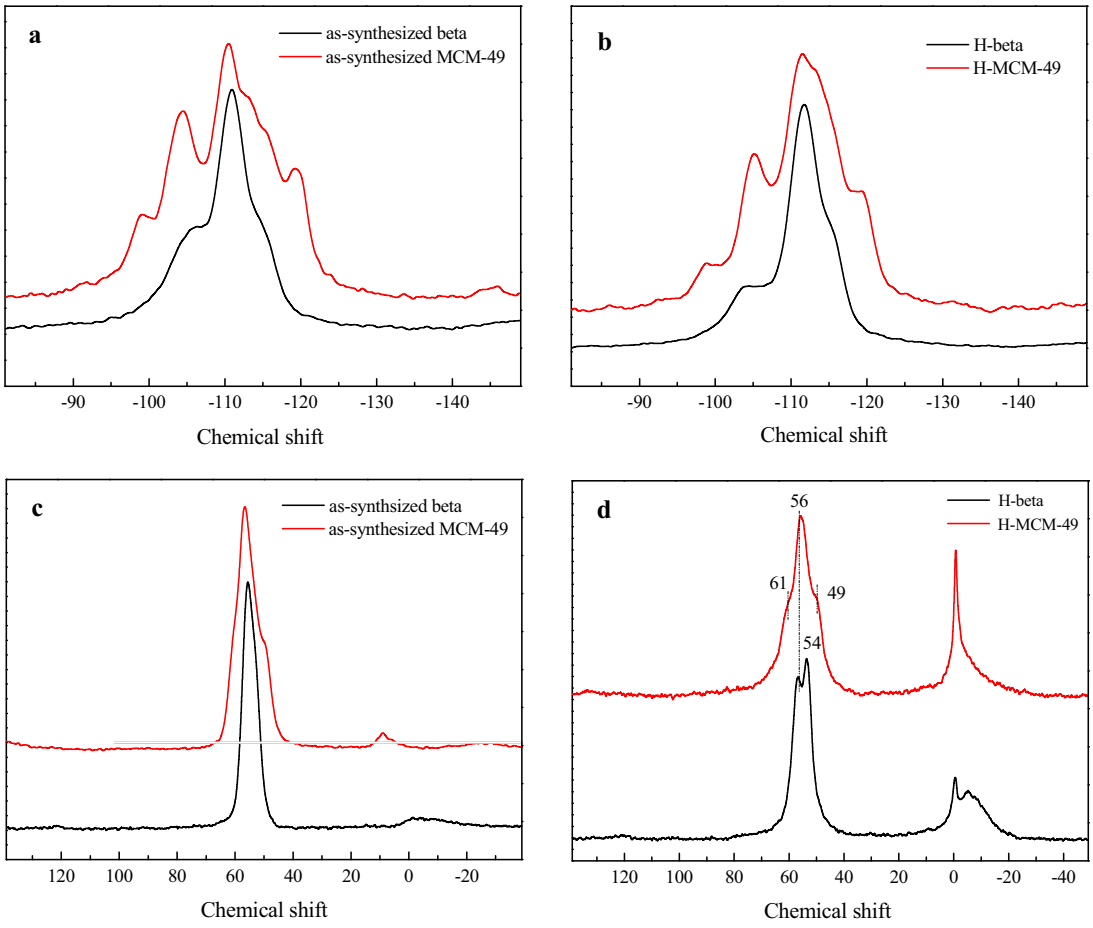

Fig. 3. $^{29}Si/^{27}Al$ MAS NMR spectra of as-synthesized and H-type zeolites.

Table 3
Acid properties of H-type zeolites.

	200 °C			350 °C		
	Lewis acid (μmol g^{-1})	BrÖnsted acid (μmol g^{-1})	B/L	Lewis acid (μmol g^{-1})	BrÖnsted acid (μmol g^{-1})	B/L
H-beta	271	423	1.50	227	396	1.74
H-MCM-49	189	402	2.13	168	375	2.23

Table 4
the sizes of reactants, product, base probes and zeolitic channels.

Samples	Kinetic diameter (nm)						
	Ethylene	Benzene	EB	Transitional state intermediate	NH_3	Pyridine	2,4,6-Trimethyl-pyridine
	0.39	0.58	0.58	0.58 < d < 0.97	0.26	0.58	0.74
H-beta							
12 MR channels (0.66 nm × 0.67 nm & 0.56 nm × 0.56 nm)	√	√	√	√	√	√	√
	√	√	√	√	√	√	√
H-MCM-49							
12 MR cups (0.71 nm × 0.71 nm × 0.91 nm)	√	√	√	√	√	√	√
12 MR supercages via 10 MR windows (0.41 nm × 0.54 nm & 0.41 nm × 0.59 nm)	√	√	√	√	√	√	
10 MR channels (0.41 nm × 0.54 nm & 0.41 nm × 0.59 nm)	√	√	√		√	√	

The sizes of pore and channel are referenced from [40].

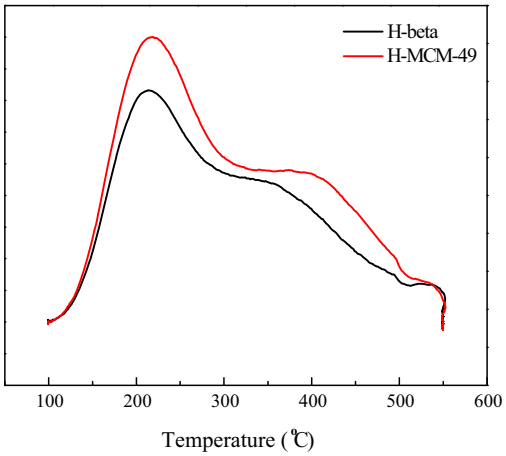

Fig. 4. NH_3-TPD curves of H-beta and H-MCM-49.

cally adsorbed 2,4,6-trimethyl-pyridine with bands at ~1485 and ~1395 cm^{-1} on the inner surface of H-beta due to activation effects of zeolitic channels on guest molecules [39]. However 2,4,6-trimethyl-pyridine cannot penetrate the inner channels of H-MCM-49 (10 MR channels and 12 MR supercages with 10 MR windows) [20,26–28]. Meanwhile physically adsorbed 2,4,6-trimethyl-pyridine could be easily desorbed under treating conditions of FTIR, therefore there were no physically adsorbed bands of 2,4,6-trimethyl-pyridine detected over H-MCM-49. According to the height of adsorption band (~1633 cm^{-1}), the amount of 2,4,6-trimethyl-pyridinewas calculated to give the accessibility of active centers, 34.9 μmol g^{-1} for H-MCM-49 and 52.7 μmol g^{-1} for H-beta. Clearly H-beta shows more acid sites accessed by 2,4,6-trimethyl-pyridine by about 51% than H-MCM-49. In the case of H-beta's three-dimensional 12 MR pore systems, an easy penetration of 2,4,6-trimethyl-pyridine into its pores led to complete disappearance of the OH acidic band at ~3610 cm^{-1} observed. However, for H-MCM-49, the slight decrease in the intensity of the acidic OH band at ~3610 cm^{-1} indicates that only a small part of acid sites could be assessed by 2,4,6-trimethyl-pyridine. According to previous results, 2,4,6-trimethyl-pyridine could only detect acid sites residing in 12 MR cups on the outer surface of H-MCM-49.From the view of reactant selectivity, the more acid sites accessed by 2,4,6-trimethyl- pyridine, the better catalytic activity in liquid-phase alkylation of benzene with ethylene.

3.3. *Alkylation performances over H-beta and H-MCM-49 catalysts*

Usually the ethylene conversion is almost 100% to ensure no ethylene to enter *trans*-alkylation reactor in industrial unit. If there was unconverted ethylene, fast deactivation will happen on ethylation and *trans*-alkylation catalysts. Also with benzene/ethylene ratio at 12, which is similar to that of single ethylation stage with multi-ethylene feeding points, is enough to guarantee the solution of ethylene in the benzene. The catalytic alkylation of benzene over H-beta and H-MCM-49 catalysts is shown in Fig. 6. Clearly, H-beta presented superior activity with ethylene conversion at 100% in the temperature range from 200 to 260 °C, but a slight decrease in EB selectivity. As for H-MCM-49, there was a stepwise increase of ethylene conversion from 96.6% at 200 °C to 99.2% at 260 °C, which indicated diffusion limits may be one of the key factors to impact the activity. Similar to H-beta, a slight decrease in EB selectivity was also observed over H-MCM-49 from 95.4% at 200 °C to 94.9% at 260 °C. On the whole, H-beta exhibits better activity but poorer EB selectivity. Regardless of lower ethylene conversion, H-

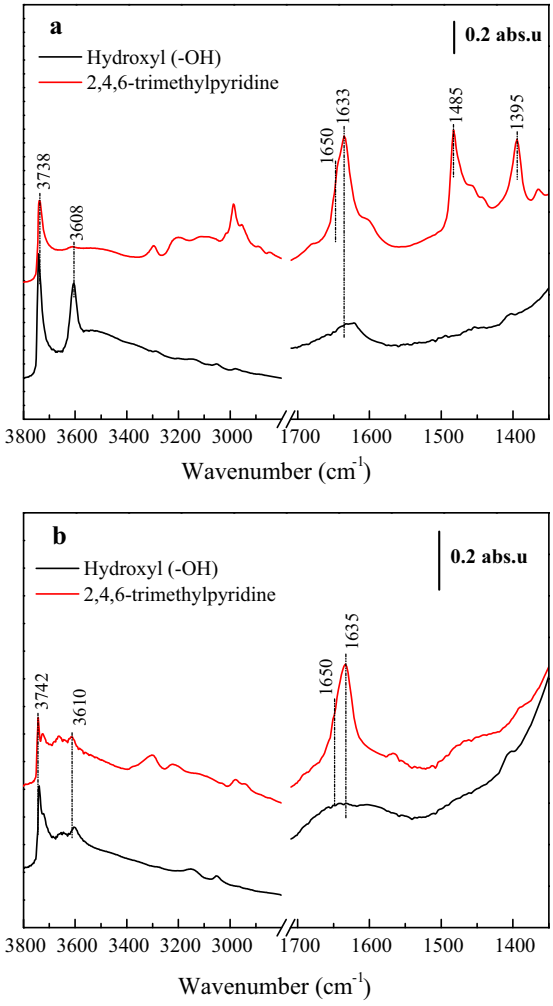

Fig. 5. 2,4,6-Trimethylpyridine spectra of H-beta (a) and H-MCM-49 (b).

MCM-49 is considered as a promising catalyst for liquid-alkylation of benzene with ethylene due to its better EB selectivity, which may lead to less energy consumption at lower benzene/ethylene ratio. Better EB selectivity means that less DEBs and TEBs were produced over H-MCM-49 than H-beta (Fig. 6c and d). The distributions of DEBs over these two catalysts are shown in Fig. 6e. The high degree of selectivity over H-MCM-49 for *o*-DEB is interesting. The kinetically favorable *o*-DEB was firstly generated and then transformed into the more thermodynamically favorable *m*-DEB. For H-beta, with the rise of temperature, thermodynamic equilibrium distributions of three DEB isomers could be approached *m*(*m*-DEB):m(*p*-DEB):m(*o*-DEB) = 64:30:6 [20]. However, for the thermodynamic equilibrium distributions over H-MCM-49 cannot be reached even at 260 °C, which was also evidence of lower isomerization activity over H-MCM-49. With ethylation selectivity considered, H-MCM-49 showed no poorer results than H-beta (Fig. 6f).

The difference in alkylation performances depends on sizes of reactant/transition-state/product and zeolite pore systems based upon shape selectivity (Table 4). Benzene (0.58 nm) could penetrate the 12 MR channels of H-beta (0.66 nm × 0.67 nm & 0.56 nm × 0.56 nm), and more importantly the12 MR pore channels of H-beta are large enough to accommodate the formation of transition state. Therefore, liquid-alkylation of benzene with ethylene over H-beta is recognized as the inner channels reaction with better accessibility of active centers, which was strongly supported by the strong adsorption of 2,4,6-trimethyl-pyridine and

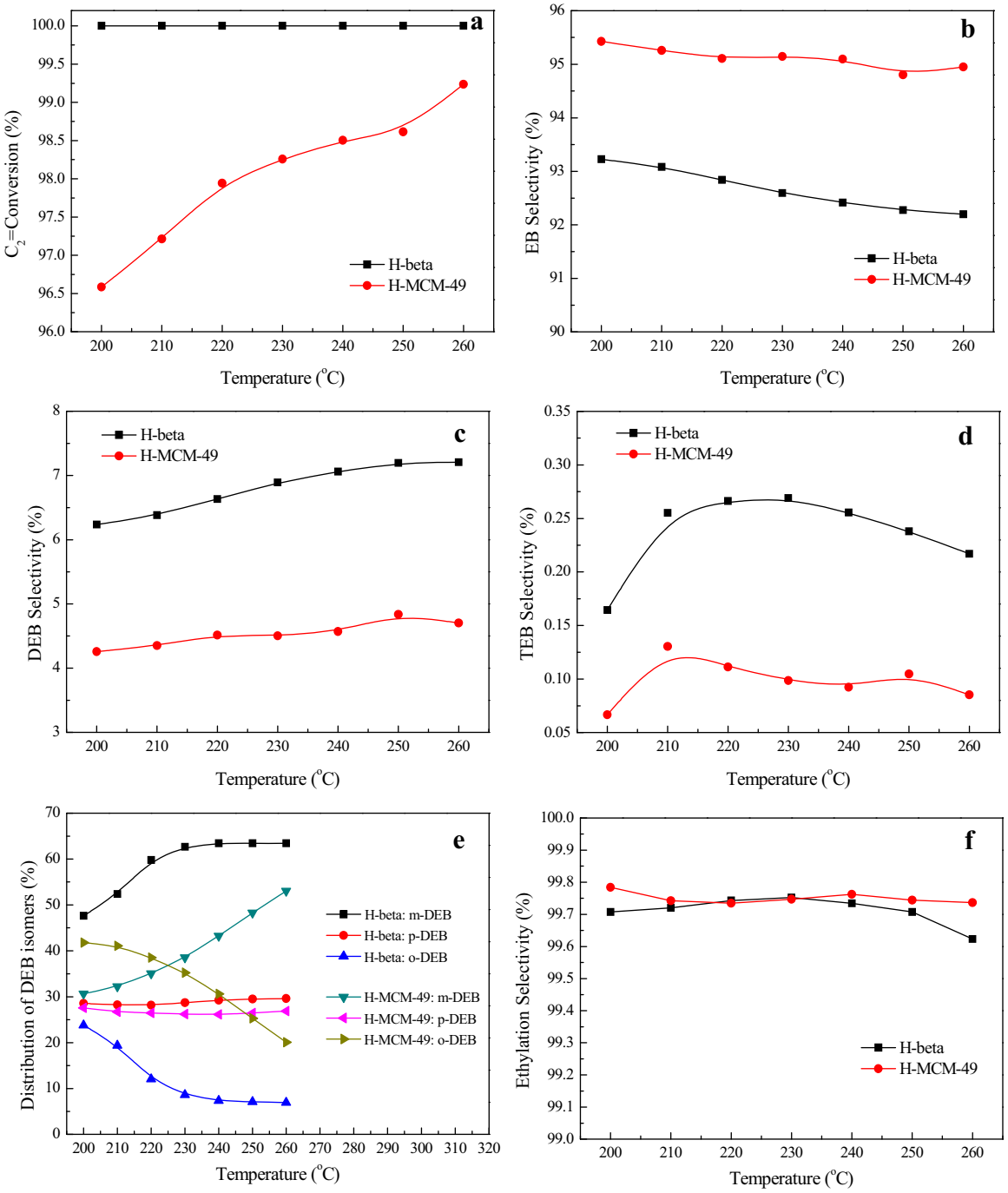

Fig. 6. Liquid-phase alkylation of benzene with ethylene over H-beta and H-MCM-49 (Liquid-phase alkylation conditions: 8 mL catalysts, T = 200–260 °C, p = 3.5 MPa, benzene WHSV^{-1} = 3.0 h^{-1}, benzene/ethylene molar ratio = 12.0).

the complete disappearance of the OH acidic band at 3610 cm^{-1}. Meanwhile for reactions proceeded in the inner channels of zeolites, guest molecules including reactants and base probes could be activated by zeolitic channels due to the negative charge of zeolitic framework. This hypothesis is also proven by strong physically adsorbed 2,4,6-trimethyl-pyridine in the pores of H-beta, which is more difficult to be desorbed than H-MCM-49. In such a way, easy diffusion into confined space in beta channels, sufficient accommodation for the transition states and activation of guest molecules by zeolitic channels are the key to superior activity over H-beta, however superior activity is not the only consideration especially for a consecutive reaction with intermediate product as the target product. Usually for a consecutive reaction, the decrease of intermediate product selectivity is usually accompanied by the increase of conversion [41,42]. For H-beta, longer diffusion distance out of confined space in inner channels surely would drive ethylation forward to the formation of DEBs and TEBs, which may be the real reason for the lower EB selectivity. Therefore as for H-beta, enhancement in EB selectivity should be given the priority rather than activity through synthesizing nano or hierarchical beta to decease the diffusion length out of confined space in inner channels.

While for H-MCM-49, things become more complicated due to three different pore systems. Although there are abundant acid sites

inside the 10 MR channels, they seem to contribute little to EB formation, which has been proven in many publications [20,26–28]. Both benzene (0.58 nm) and ethylene can penetrate the 10 MR channels. Also it has been extensively proven that 10 MR channels are large enough to accommodate benzene, ethylbenzene even *p*-DEB [20]. However there are insufficient spaces to accommodate the transition state during formation of EB, i.e., transition state selectivity. Also some reports have claimed that active centers useful for EB synthesis were mainly located in 12 MR cups on the external surface of MWW zeolites, which does not restrict the diffusion of reactant/transition state/product toward/from the active centers [20,26–28]. 2,4,6-Trimethyl-pyridine can only be adsorbed on the acid sites located in the 12 MR cups on the outer surface of H-MCM-49 with little restriction on the reactants and EB, indicating less chances to be further ethylated to form DEBs and TEBs. Different from confined spaces in the channels of beta catalyst, 12 MR cups on the external surface of MWW catalysts could be viewed as open space for catalysis i.e. surface pocket catalysis. Poor activation of guest molecules by open space of 12 MR cups of MWW zeolite than inner channels of beta zeolite may lead to inferior activity. However open space of 12 MR cups accounts for higher EB selectivity over MWW catalysts because of easy escaping from acid sites to avoid further alkylation. As for 12 MR supercages with 10 MR windows, there are few reports on its influences on activity and selectivity in liquid-phase alkylation of benzene with ethylene. Benzene and ethylene could penetrate 12 MR supercages through 10 MR windows, and 12 MR supercages are large enough to form the transition state of EB. The key lies in the poorer diffusion of benzene into of 12 MR supercages through 10 MR windows, which led to a stepwise increase of ethylene conversion from 200 to 260 °C. There has been several reports confirmed our proposal that 12 MR supercages could catalyze alkylation of benzene even with long chain alkenes [43,44]. The other issue is selectivity. Although the kinetic diameters of EB is similar to benzene at about 0.58 nm, EB molecules show poorer diffusion capability than benzene due to the ethyl group, which usually caused the formation of DEBs, TEBs and heavier aromatics resulting in poorer EB selectivity and deactivation. The 12 MR supercages also contribute to the fast deactivation of catalysts especially in alkylation of longer chain alkenes [44]. The reason also lies in the poor diffusion of products out of 12 MR supercages through 10 MR windows. With more supercages, Y zeolite suffered a much faster deactivation and poorer selectivity regardless of 12 MR windows [20].

In our recent paper, it has been proven that liquid-phase alkylation of benzene with ethylene over MWW zeolites is an inner diffusion-limited reaction. With the decrease of MWW crystal sizes, the ethylene conversion and EB selectivity could be simultaneously increased [45]. Extreme condition of inner diffusion is considered as the external surface reaction, strongly supporting previous proposal that liquid-phase alkylation of benzene with ethylene over MWW zeolites is the external surface reaction [20,28,38]. Conventionally active centers useful for EB synthesis are thought to locate in 12 MR cups on the external surface of MWW zeolites, which do not restrict the diffusion of reactants/products toward/from the active centers [20]. That is to say, most of acid sites residing in the inner 10 MR channels are not utilized during the liquid-phase alkylation of benzene with ethylene, and cannot be utilized because of transition state selectivity. As concluded in this paper, the key to increase the alkylation performances of MWW zeolites is to increase the diffusion of benzene/EB into/out of 12 MR supercages through 10 MR windows, equal to increase the activity/selectivity of this reaction. According to reports, the acid sites on the external surface of MWW zeolites account for less than 15% of total acid sites, that is, only a small portion is utilized in the liquid-phase alkylation of benzene with ethylene [20,26–28], which also leads to poorer activity over MWW zeolite than beta. Therefore, to enhance activity without loss of EB selectivity over MWW zeolites, much attention should be put into promoting the diffusion through 10 MR windows governing 12 MR supercages. It has been proven that 3D structure of MWW zeolite could be changed to corresponding lamellar precursor via a reversible rearrangement in presence of HMI or piperidine, which returned reversibly to the 3D MWW structure by further calcination [46,47]. We have reported to tailor the aggregation of MWW layers, crystals and particles to improve accessibility of active centers (one supercage is divided into two 12 MR cups) via synthesis of MCM-56, directing-gel method, zeolite–zeolite transformation and post-synthesis to improve catalytic performances in liquid-phase alkylation of benzene with ethylene [45,48–52]. In future research, the degree of 12 MR supercages splitting into 12 MR cups should be assessed and adjusted.

4. Conclusion

Based upon the shape selectivity, comprehensive research were conducted on acidity characterization and catalytic performance in liquid-phase alkylation of benzene with ethylene over *BEA and MWW zeolites. According to reactant selectivity, H-beta and H-MCM-49 were characterized by base probes with different molecule sizes. NH_3, pyridine and 2,4,6-trimethyl-pyridine could penetrate H-beta channels to access the acid sites. Although both NH_3 and pyridine could detect the acid sites on internal and external surface of H-MCM-49, 2,4,6-trimethyl-pyridine, which could dominantly be adsorbed on the acid sites located in 12 MR cups on the outer surface of H-MCM-49, gave less number of acid sites than H-beta. Based on the sizes of base probes/reactants/transition states/products/pore channels, the difference in catalytic performance over H-beta and H-MCM-49 was summarized. Easy diffusion into confined spaces and activation of reactant molecules by zeolitic channels accounts for superior activity, however longer diffusion distance for EB escaping results in poor EB selectivity. Therefore as for H-beta, enhancement in EB selectivity should be given the priority rather than activity through synthesizing nano or hierarchical beta to decease the diffusion length out of confined space in inner channels. As for H-MCM-49, acid sites located in 10 MR channels contributed little to the formation of EB due to transition state selectivity. Acid sites located in 12 MR cups on the external surface of MWW zeolites with little restriction on the diffusion of reactant/product toward/from the active centers were the major active centers for EB formation. However the acid sites on the outer surface of H-MCM-49 only accounted for a small part of total acid sites, which could be determined by 2,4,6-trimethyl-pyridine. Therefore, to enhance activity without loss of EB selectivity over MWW zeolites, much attention should be put into promoting the diffusion through 10 MR windows governing 12 MR supercages, i.e. transforming confined space (12 MR supecages) into open space (12 MR cups).

Acknowledgments

This work was supported by the National Basic Research Program of China (973 Program, No. 2012CB224805). Special thanks to the Department of Analysis in Research Institute of Petroleum Processing Sinopec.

References

[1] C. Perego, P. Ingallina, Catal. Today 73 (2002) 3–22.
[2] G. Bellussi, A. Carati, C. Rizzo, R. Millini, Catal. Sci. Technol. 3 (2013) 833–857.
[3] V.J. Frilette, P.B. Weisz, R.L. Golden, J. Catal. 1 (1962) 301–306.
[4] P.B. Weisz, V.J. Frilette, J. Phys. Chem. 64 (1960) 382–383.
[5] S. Teketel, L.F. Lundegaard, W. Skistad, S.M. Chavan, U. Olsbye, K.P. Lillerud, P. Beato, S. Svelle, J. Catal. 327 (2015) 22–32.
[6] B. Yilmaz, U. Muller, Top. Catal. 52 (2009) 888–895.

[7] R. Gounder, E. Iglesia, Acc. Chem. Res. 45 (2012) 229–238.
[8] U. Olsbye, S. Svelle, M. Bjorgen, P. Beato, T.V.W. Janssens, F. Joensen, S. Bordiga, K.P. Lillerud, Angew. Chem. Int. Ed. 51 (2012) 5810–5831.
[9] P. Matias, J.M. Lopes, S. Laforge, P. Magnoux, P.A. Russo, M.M.L. Ribeiro Carrott, M. Guisnet, F.R. Ribeiro, J. Catal. 259 (2008) 190–202.
[10] J. Rigoreau, S. Laforge, N. Gnep, M. Guisnet, J. Catal. 236 (2005) 45–54.
[11] B. Onida, F. Geobaldo, F. Testa, F. Crea, E. Garrone, Microporous Mesoporous Mater. 30 (1999) 119–127.
[12] D. Meloni, S. Laforge, D. Martin, M. Guisnet, E. Rombi, V. Solinas, Appl. Catal. A: Gen. 215 (2001) 55–66.
[13] J. Cejka, B. Wichterlova, Catal. Rev. Sci. Eng. 44 (2002) 375–421.
[14] S. Al-Khattaf, S.A. Ali, A.M. Aitani, N. Zilkova, D. Kubicka, J. Cejka, Catal. Rev. Sci. Eng. 56 (2014) 333–402.
[15] B. Zhang, Y.J. Ji, Z.D. Wang, Y.M. Liu, H.M. Sun, W.M. Yang, P. Wu, Appl. Catal. A: Gen. 443–444 (2012) 103–110.
[16] G. Bellussi, G. Pazzuconi, C. Perego, G. Girotti, G. Terzoni, J. Catal. 157 (1995) 227–234.
[17] Y.C. Du, H. Wang, S. Chen, J. Mol. Catal. A: Chem. 179 (2002) 253–261.
[18] J.C. Cheng, C.M. Smith, D.E. Walsh, Alkylation of Benzene with Ethylene, US 5493065 (1996).
[19] J.C. Cheng, C.M. Smith, C.R. Venkat, D.E. Walsh, US 5600048 (1997).
[20] J. Cheng, T. Degnan, J. Beck, Y. Huang, M. Kalyanaraman, J. Kowalski, C. Loehr, D. Mazzone, Stud. Surf. Sci. Catal. 121 (1999) 53–60.
[21] D.Y. Jan, J.A. Johnson, R.J. Schmidt, G.B. Woodle, US 7268267 B2 (2007).
[22] W.J. Roth, J. Cejka, Catal. Sci. Technol. 1 (2011) 43–53.
[23] S.L. Lawton, A.S. Fung, G.J. Kennedy, L.B. Alemany, C.D. Chang, G.H. Hatzikos, D.N. Lissy, M.K. Rubin, H.K.C. Timken, S. Steuernagel, D.E. Woessner, J. Phys. Chem. 100 (1996) 3788–3798.
[24] W.J. Roth, D.L. Dorset, Microporous Mesoporous Mater. 142 (2011) 32–36.
[25] L.M. Rohde, G.J. Lewis, M.A. Miller, J.G. Moscoso, J.L. Gisselquist, R.L. Patton, S.T. Wilson, D.Y. Jan, US 6756030 B1 (2004).
[26] H. Du, D.H. Olson, J. Phys. Chem. B. 106 (2001) 395–400.
[27] P. Ayrault, J. Datka, S. Laforge, D. Martin, M. Guisnet, J. Phys. Chem. B. 108 (2004) 13755–13763.
[28] S.H. Cha, J. Lee, J. Shin, S.B. Hong, Top. Catal. 58 (2015) 537–544.
[29] E.H. Xing, X.Z. Gao, W.H. Xie, F.M. Zhang, X.H. Mu, X.T. Shu, RSC Adv. 4 (2014) 24893–24899.
[30] E.H. Xing, Y.C. Shi, W.H. Xie, F.M. Zhang, X.H. Mu, X.T. Shu, RSC Adv. 5 (2015) 8514–8522.
[31] A.L.S. Marques, J.L.F. Monteiro, H.O. Pastore, Microporous Mesoporous Mater. 32 (1999) 131–145.
[32] D. Vuono, L. Pasqua, F. Testa, R. Aiello, A. Fonseca, T.I. Koranyi, J.B. Nagy, Microporous Mesoporous Mater. 97 (2006) 78–87.
[33] R. Ravishankar, T. Sen, V. Ramaswamy, H.S. Soni, S. Ganapathy, S. Sivasanker, Stud. Surf. Sci. Catal. 84 (1994) 331–338.
[34] A. Corma, C. Corell, J. Pérez-pariente, Zeolite 15 (1995) 2–8.
[35] W. Kolodziejski, C. Zicovich-Wilson, C. Corell, J. Pérez-pariente, A. Corma, J. Phys. Chem. 99 (1995) 7002–7008.
[36] M.A. Camblor, A. Corma, S. Valencia, Microporous Mesoporous Mater. 25 (1998) 59–74.
[37] B. Gil, W. Makowski, B. Marszalek, W.J. Roth, M. Kubu, J. Cejka, Z. Olejniczak, Dalton Trans. 43 (2014) 10501–10511.
[38] F. Thibault-Starzyk, A. Vimont, J. Gilson, Catal. Today 70 (2001) 227–241.
[39] B.L. Bleken, L. Mino, F. Giordanino, P. Beato, S. Svelle, K.P. Lilleruda, S. Bordiga, Phys. Chem. Chem. Phys. 15 (2013) 13363–13370.
[40] C. Baerlocher, L.B. McCusker, D.H. Olson, Atlas of Zeolite Framework Types, sixth edition, Elsevier, 2007.
[41] J.G. Van de Vusse, Chem. Eng. Sci. 21 (1966) 1239–1252.
[42] L.D. Schemidt, The Engineering of Chemical Reactions, University Press, New York, Oxford, 1998, pp. 157.
[43] K.F. Liu, S.J. Xie, S.L. Liu, G.L. Xu, N.N. Gao, L.Y. Xu, J. Catal. 283 (2011) 68–74.
[44] H.T. Yen, J.J. Wang, S.H. Siao, S.H. Cha, S.B. Hong, S.S. Al-Khattaf, I. Wang, T.C. Tsai, Catal. Sci. Technol. (2016), http://dx.doi.org/10.1039/c5cy02208h, Advance article.
[45] Y.C. Shi, E.H. Xing, X.Z. Gao, D.Y. Liu, W.H. Xie, F.M. Zhang, X.H. Mu, X.T. Shu, RSC Adv. 5 (2015) 13420–13429.
[46] L.L. Wang, Y.M. Liu, W. Xie, H.H. Wu, X.H. Li, M.Y. He, P. Wu, J. Phys. Chem. C 12 (2008) 6132–6138.
[47] Y.J. Ji, H. Xu, D.R. Wang, L. Xu, P. Ji, H.H. Wu, P. Wu, ACS Catal. 3 (2013) 1892–1901.
[48] E.H. Xing, Y.C. Shi, W.H. Xie, F.M. Zhang, X.H. Mu, X.T. Shu, RSC Adv. 6 (2016) 29707–29717.
[49] Y.C. Shi, E.H. Xing, W.H. Xie, F.M. Zhang, X.H. Mu, X.T. Shu, Microporous Mesoporous Mater. 215 (2015) 8–19.
[50] E.H. Xing, Y.C. Shi, A.G. Zheng, J. Zhang, X.Z. Gao, D.Y. Liu, M.D. Xin, W.H. Xie, F.M. Zhang, X.H. Mu, X.T. Shu, Ind. Eng. Chem. Res. 54 (2015) 3123–3135.
[51] Y.C. Shi, E.H. Xing, W.H. Xie, F.M. Zhang, X.H. Mu, X.T. Shu, Appl. Catal. A: Gen. 497 (2015) 135–144.
[52] Y.C. Shi, E.H. Xing, W.H. Xie, F.M. Zhang, X.H. Mu, X.T. Shu, Microporous Mesoporous Mater. 220 (2016) 7–15.